CHEMISTRY & CHEMICAL TECHNOLOGY

Vol. 10, No. 4, 2016 Chemistry

Hanane Fodil and Mahmoud Omari

SYNTHESIS, STRUCTURAL AND PHYSICOCHEMICAL CHARACTERIZATION OF $BaFe_{1-X}Al_XO_{3-\Delta}$ OXIDES

Laboratory of Molecular Chemistry and Environment, University of Biskra, B. P. 145, 07000 Biskra, Algeria; ha.fodil@yahoo.fr

Received: January 29, 2016 / Revised: February 22, 2016 / Accepted: June 12, 2016

Abstract. In this study, $BaFe_{1-x}Al_xO_{3-\delta}$ ($0 \leq x \leq 0.3$) perovskite-type oxides were prepared by sol-gel method using citric acid as chelating agent. The samples were subjected to various calcination temperatures in order to investigate the physicochemical properties of the oxide affected by the parameter. Thermogravimetric analysis, Fourier transform infrared spectroscopy and X-ray diffraction (XRD) techniques are used to explore precursor decomposition and to establish adequate calcination temperature for the preparation of the nano-powders. The studied compounds have hexagonal crystal structure at the temperature of 1123 K. The samples obtained after calcination at 1123 K were characterized by XRD, Brunauer-Emmett-Teller surface area analysis, scanning electron microscopy, powder size distribution and electrical conductivity. The microstructure and morphology of the compounds show that the particles are nearly spherical in shape and are partially agglomerated. The highest surface area and total pore volume are achieved for $BaFe_{0.8}Al_{0.2}O_{3-\delta}$ oxide. Temperature dependence of electrical conductivity shows a semiconducting behavior.

Keywords: perovskite oxide, BET, sol-gel method, powder diffraction, electrical conductivity.

1. Introduction

In recent years, there has been a continuous interest in developing new materials with perovskite structure. Perovskite oxides have the general formula ABO_3, where the B-site cation occupies the interstitial site of an octahedron of oxygen anions and the A-site cation fits in the large cavity at the centre of the 12 coordination site [1, 2]. Showing a wide range of oxygen stoichiometry, these materials have been attracting much attention due to the existence of mixed ionic and electronic conductivity, and find application in several fields such as catalysis, fuel cells, oxygen sensors, and membranes for gas separations [3, 4]. It has been demonstrated that the existence of mixed valence states of the B ion plays an essential role in determining the physical properties of this kind of materials [5].

Perovskite $BaFeO_{3-\delta}$ is an interesting material which exhibits high mixed oxide ionic and electronic conductivity and therefore can be potentially used in electrochemical devices such as oxygen permeation membranes, oxygen sensors, and SOFCs [6-8]. It is also an instructive model whose crystal structure and electronic properties are sensitively related to the oxygen vacancy ordering. Fe cations in this system are in a mixed valence state ranging from +4 to +3, corresponding to a wide range of oxygen non stoichiometry (from 0 to 0.5). These complex oxides can be properly modified by the partial substitution of atoms at A and/or B sites, which may strongly affect their physical properties. Indeed, depending on the doping component and level, the material can display ferromagnetic or thermo-electrical properties [9, 10] and electrochemical properties [11, 12]. $BaFeO_{3-\delta}$ doped with various metal ions such as Nb [13], Ca [14], Co [12], Ca and Co [15], were previously studied. These oxides have been identified as promising IT-SOFC cathode materials and oxygen transport membranes.

A few years ago, several studies have shown that the isovalent doping into the Fe sublattice with trivalent cations having stable oxidation state, such as Ga or Al, enhance the stability of perovskite ferrite [16-18]. On the other hand, another work on Al-doped perovskite anodes for oxidation of hydrogen in IT-SOFC has been carried out [18]. It has been revealed that suitable power densities of about 420 mW/cm^2 for the direct oxidation of hydrogen were achieved at 1073 K.

Despite these advantages, there have been no reports to date concerning the synthesis and characterization of aluminium doped barium ferrite

oxides. In our present work, samples of the $BaFe_{1-x}Al_xO_{3-\delta}$ (x = 0, 0.1, 0.2 and 0.3) system were synthesized in order to evaluate the influence of the amount of aluminium on the thermal and structural properties of the system. The synthesis was carried out by the citric acid sol-gel method using absolute formaldehyde (methanal) as solvent, and characterized by X-ray diffraction (XRD), Brunauer-Emmett-Teller specific surface area (S_{BET}) analysis, infrared spectroscopy (IR), scanning electron microscopy, thermal analysis (TGA), powder size distribution (PSD), and electrical conductivity.

2. Experimental

2.1. Synthesis

$BaFe_{1-x}Al_xO_{3-\delta}$ oxides with ($0 \leq x \leq 0.3$) were prepared by a sol-gel method using citric acid as a complexing agent. Aqueous solutions of $Ba(NO_3)_2$ (PANREAC 99 %), $Fe(NO_3)_3{\cdot}9H_2O$ (BIOCHEM 98.5 %), and $Al(NO_3)_3{\cdot}9H_2O$ (BIOCHEM 99 %) were first dissolved in absolute formaldehyde (methanal) separately. The molar amount of citric acid was equal to total molar amount of metal nitrates in solution. Citric acid (Biochem) was added to the precursors under vigorous stirring. The homogeneous solution obtained was heated at 353–363 K for 4 h. To remove the solvent, the gel is heated for 24 h at 373 K. The resulting precursor is then milled and calcined in air for 6 h at different calcination temperatures: 673, 873, 973, 1073, 1123, 1173, 1223, and 1273 K with the heating rate of 5 $K{\cdot}min^{-1}$.

2.2. Characterization Techniques

The thermal decomposition processes of the precursor gels were studied in air atmosphere by TGA Schimadzu with a heating rate of 10 K/min in air, from room temperature to 1273 K.

Infrared transmission spectra were performed on a Fourier transform spectrometer (FTIR) Shimadzu 8400S. A granular technique employing KBr (1 mg of sample added to 200 mg of KBr) was used, and the spectra were recorded in the 400–1300 cm^{-1} range.

XRD patterns were collected on a Bruker AXS D8 advance diffractometer employing Cu Ka radiation. In all diffractograms, a step size of 0.02° ($2q$) was used with a data collection time of 15 s. Data were collected between $2q$ values of 10° and 80° using standard $q/2q$ geometry. Identification of crystalline phases was carried out by comparison with JCPDS standards. The unit cell parameters were obtained by fitting the peak position of the XRD pattern using the CELREF and X'pert Highscore programs. Moreover, morphological aspects of the powders were examined by using an ESEM-FEI Quanta 600 FEG scanning electron microscope.

The analysis of the distribution of the grain size of the samples was employed in order to show the influence of the Fe/Al substitution and the synthetic method employed on the particle size by laser granulometry. After calcination at 1123 K, the powder was dispersed in deionized water in a beaker with magnetic stirring and combined under ultrasound for 15 min. Powder size distribution (PSD) was characterized with a laser particle size analyzer (Mastersizer 2000, Malvern) [19].

The specific surface area of the samples (S_{BET}) was determined by applying the BET method to nitrogen adsorption/desorption isotherms recorded at 77 K, using a micrometrics apparatus model Nova series 2000 Quantachrome automatic sorptiometer. Prior to adsorption, the samples were degassed overnight at 433 K. Pore volume (single point adsorption total pore volume of pores less than ca. 80 nm diameter at P/Po ca. 0.98 and *t*-plot micropore volume) was also determined from corresponding analysis of the isotherms.

The electrical conductivity was measured using the standard d.c. four-probe method. The sample was heated using a cryostat (Janis Inc.). The voltage was measured using a sensitive (V-I) source (Keithley 2182) with accuracy better than 10 µV. In all measurements, the temperature was raised slowly to the required temperature at which the V-I characteristics were measured.

3. Results and Discussion

3.1. Thermogravimetric Analysis

The precursors $BaFe_{0.9}Al_{0.1}O_{3-\delta}$ (after the drying step of the preparation at 373 K) were examined by TGA in order to explore its decomposition under atmospheric air and with the aim of establishing most adequate calcination conditions. The results are shown in Fig. 1. This profile is characterized by four significant weight loss stages at the temperature ranges of 298–453, 453–623, 623–913, and 913–1203 K. The first weight loss in the temperature range 298–453 K, which must be related to desorption of adsorbed or hydration water, may remain in the precursors [20]. The second one represents an important mass loss (ca. 27 %) and takes place between ca. 453 and 623 K. Such mass loss appears consistent with the oxidative decomposition of citrates complexing the metals in the precursors [21]. The third one takes place between ca. 623 and 913 K and corresponds to the mass loss of about 17 %. It could be related to the decomposition of carbonate or carboxylate-type complexes remaining in the samples, as will be confirmed below. The final process occurs between 913 and 1203 K and must correspond to the crystallization of the oxides, as will be confirmed below, along with the slow decomposition of more persistent residual carbonate- or carboxylate-type

species [21]. Above 1203 K a slight weight loss was observed, which can be possibly attributed to the change in crystal structure, and the oxygen loss in the system.

3.2. X-ray Diffraction

XRD experiments were first performed to check the phase purity of the materials. Fig. 2 shows the XRD patterns of $BaFe_{0.9}Al_{0.1}O_{3-\delta}$ calcined at different temperatures for 6 h. After calcination at 673 and 873 K, the precursor is a mixture containing orthorhombic $BaCO_3$ (PDF:05-0378) and spinel $BaFe_2O_4$ (PDF:46-0113). When the precursor was heated over 973 K in air for 6 h, the characteristic diffraction peaks of $BaCO_3$ and $BaFe_2O_4$ decrease and become weaker at 1073 K, while those of hexagonal perovskite structure appear (PDF:01-070-0034). At 1123 K the intensity of characteristic diffraction peaks of hexagonal perovskite becomes stronger and no reflections from barium oxide are observed as distinct intermediate phases to the formation of $BaFe_{0.9}Al_{0.1}O_{3-\delta}$ during the thermal decomposition of the precursor powder. With further increase in calcination temperature above 1223 K the main intensive peak at 31° split into multiple peaks between 30.9 and 31.9° indicating the change in crystal structure, which was due to the transformation from hexagonal to rhombohedral structure (PDF:00-020-0130). This is consistent with TGA. This change should be ascribed to the oxygen loss and the formation of oxygen vacancy [20, 22].

Fig. 3 shows the XRD patterns of the $BaFe_{1-x}Al_xO_{3-\delta}$ (x = 0, 0.1, 0.2 and 0.3), sintered at 1223 K for 6 h in air. As expected, the sample with x = 0 displays the pattern of $BaFeO_{3-\delta}$ perovskite-type oxide with hexagonal symmetry, space group P63/mmc according to the standard data (PDF:01-070-0034). Additional peaks are shown to grow with increasing x, the most intense ones appearing at $2q \sim 28.2$ and 33.4°, which correspond to orthorhombic $BaFe_2O_4$ (JCPDS No. 46-0113). Besides, owing to the instability of Fe^{4+} in $BaFeO_{3-\delta}$ oxide, under the air atmosphere calcination in which the oxygen is not sufficient, we can see also micro amount of $BaFe_2O_4$ phases containing Fe^{3+}. A similar observation was found in $BaFe_{1-x}Ti_xO_{3-\delta}$ [23] and $Ba(Fe,Co)O_{3-\delta}$ [12]. Fe^{+4} as observed in similar perovskite-type oxide [24, 25]. Several authors have ascribed this feature to indicate the presence of Fe^{4+} [24-26]. Yoon and Kim [26] demonstrated with the help of chemical analysis and Mossbauer spectroscopy employed on $La_{1/3}Sr_{2/3}FeO_3$ that it was hard to single out the absorption line from the Mossbauer spectra and even the chemical analysis definitely pointed out the presence of Fe^{4+}. Bellaki *et al.* [27] also observed Fe^{4+} in $LaFeO_3$ with the help of iodometric titration. Iodometric titration and temperature programmed reduction carried out by Falcon *et al.* [28] on $LaFeO_3$ evidenced the simultaneous presence of iron in Fe^{4+} state and excess oxygen. These all findings support the presence of Fe^{4+} in the investigated systems.

A shift to lower angle of the peaks of this perovskite phase observed upon increasing x (Fig. 4), is due to the incorporation of aluminum ions with a great ionic radius in comparison with Fe.

The lattice parameters of the perovskites $BaFe_{1-x}Al_xO_{3-\delta}$ were calculated for each x value from the XRD patterns using Celref program. The values of a and c cell parameters (Å) *vs*. the degree of substitution x are summarized in Table 1. We observe that both parameters and volume increase with increasing Al content in the samples. This feature is explained considering that smaller Fe^{3+} ions are substituted by bigger Al species in the octahedral sites of the perovskite frame work (ionic radius of Al^{3+} (CN:XI) and Fe^{3+} (CN:XI) are equal to 0.605 and 0.585 Å, respectively [23, 29]. The unit cell volume as a function of Al content after treating the samples in air is shown in Fig. 5. The lattice volume change does not follow Vegard's law. This disagreement suggests a more complex structure than a simple solid solution.

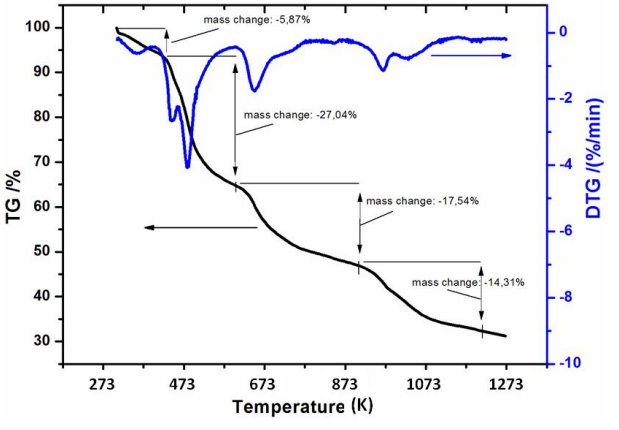

Fig. 1. Thermogravimetric profiles of $BaFe_{0.9}Al_{0.1}O_{3-\delta}$ precursor heated in air at 10 K min^{-1}

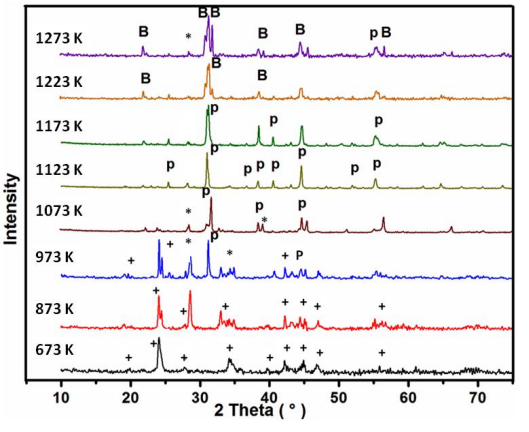

Fig. 2. XRD patterns of the $BaFe_{0.9}Al_{0.1}O_{3-\delta}$ powder calcined at different temperatures: $BaCO_3$ (+); $BaFe_2O_4$ (*); hexagonal phase (P) and rhombohedral phase (B)

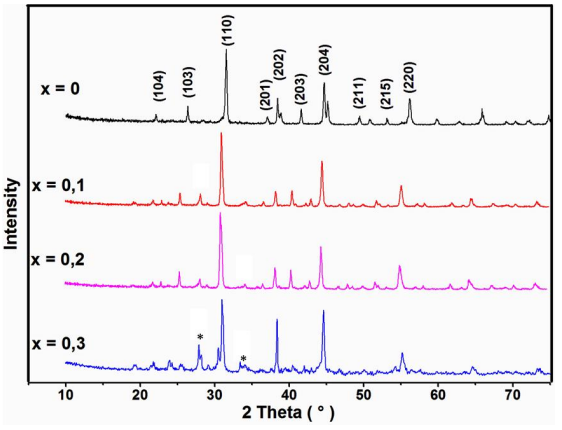

Fig. 3. XRD patterns of the $BaFe_{1-x}Al_xO_{3-\delta}$ ($0.0 \leq x \leq 0.3$) samples calcined at 1123 K: $BaFe_2O_4$ (*)

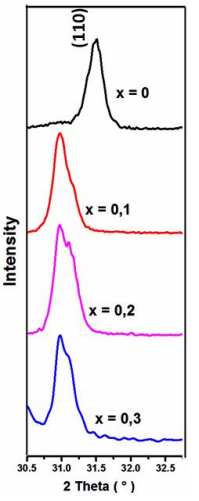

Fig. 4. Evolution of the position of the highest X-ray diffraction peak

Table 1

Values of unit cell parameters for pure and substituted $BaFeO_{3-\delta}$

Nominal compositions	$a = b$, Å	c, Å	V, Å^3
$BaFeO_{3-\delta}$	5.6768	13.9560	389.49
$BaFe_{0.9}Al_{0.1}O_{3-\delta}$	5.7792	14.0639	406.79
$BaFe_{0.8}Al_{0.2}O_{3-\delta}$	5.7612	14.4386	415.04
$BaFe_{0.7}Al_{0.3}O_{3-\delta}$	5.7715	14.4401	417.23

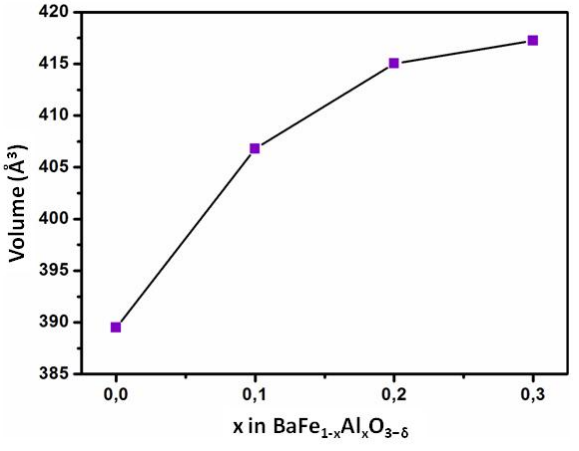

Fig. 5. Lattice volume dependence on aluminum content (x) for $BaFe_{1-x}Al_xO_{3-\delta}$

3.3. IR Spectroscopy

The chemical and structural changes that take place during combustion can be observed from the Fourier transform infrared analysis. Fig. 6 shows the FT-IR spectra of $BaFe_{0.9}Al_{0.1}O_{3-\delta}$ nanoparticles in the range of 400–1300 cm^{-1}. The dried gel and calcined at 873 and 973 K calcined samples show bands at 852 and 775 cm^{-1} corresponding to stretching vibrations of carbonate group and NO^{3-} ions, respectively [20, 22, 30]. These bands tend to disappear by increasing the post sintering temperature and completely vanished at temperatures higher than 1123 K. The disappearance of these bands reveals that the remnant carbonate and NO^{3-} ions in the samples are removed at these high temperatures. It is noticed that the broad and shallow peaks appearing around 625 and 490 cm^{-1} at lower annealing temperatures becomes sharp and intense as the annealing temperature is increased. These results are in accordance with the XRD analysis (Fig. 2). The FT-IR spectrum of $BaFe_{0.9}Al_{0.1}O_{3-\delta}$ sample annealed at 1123 K show two characteristic vibration bands at 625 and 490 cm^{-1}. These bands (625–490 cm^{-1}) are assigned to

the stretching modes of the MO_6 octahedral unit and to the deformation of this same polyhedral unit respectively [20, 22, 31]. With the calcination temperature further increasing to 1273 K, the peaks at 625 and 490 cm^{-1} become more obtuse. A scrutiny of FTIR spectra, TG and XRD patterns obtained for samples post sintered at different temperatures clearly reveals the evolution of phases and finally the formation of perovskite type barium ferrite nanograins.

3.4. Structural and Morphological Characterization

The average crystallite size (D) was evaluated from the broadening of the XRD line width by applying the Scherer's formula Eq. (1) [32]:

$$D = 0.89\, l / b \cos q \qquad (1)$$

where D is the crystallite size; λ is the wavelength of X-ray; β is the full width at half maximum (β is expressed in radians), and θ is the Bragg's angle.

The crystallite size for different compositions is presented in Fig. 7. It is observed that crystallite size decreases with increasing aluminum content. This is probably due to the incorporation of Al^{+3} into the $BaFeO_{3-\delta}$ lattice which leads to the crystallite decrease. Similar tendency has been found previously for $La_{1-x}Sr_xMnO_3$ samples synthesized by coprecipitation of precursor acetates [33] and $LaCo_{1-x}Ru_xO_3$ [34] prepared by Pechini sol-gel method.

Table 2 summarizes the basic textural properties of the samples. As noted, the S_{BET} and micropore volume of the samples monotonically increase with increasing x, while the total pore volume shows a maximum at $x = 0.2$. This latter suggests that the specific surface area can be determined by the balance between the crystal size and the degree of agglomeration of the nanocrystals in each case. The observed S_{BET} increase can in this sense be basically determined by the crystal size decrease [35].

The grain size of the different oxides calcined at 1123 K, according to PSD measurements, are shown in Fig. 8. The size distribution of the $x = 0$, 0.1, 0.2 and 0.3 samples shows a maximum at ca. 28.9, 21.2, 25.4 and 24.5 microns, respectively. Size distributions obtained with maximum at tens of microns must result from agglomeration of primary particles. The decrease in the particle size observed upon increasing x contrasts with the evolution observed in S_{BET} values (Table 2). Crystal size estimate from use of the Scherrer equation for the major perovskite phase is of 59.8, 52.7, 50.2 and 50.6 nm for $x = 0$, 0.1, 0.2 and 0.3, respectively. No direct correlation can be established between these values and those of S_{BET} and pore volumes or grain sizes (Table 2; Fig. 8), suggesting that the specific surface area becomes basically determined by morphological properties of the Al doped $BaFeO_{3-\delta}$ nanoheterostructures formed in each case.

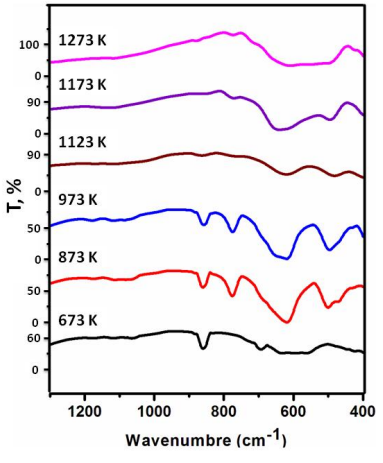

Fig. 6. Infrared spectra of $BaFe_{0.9}Al_{0.1}O_{3-\delta}$ calcined at different temperatures

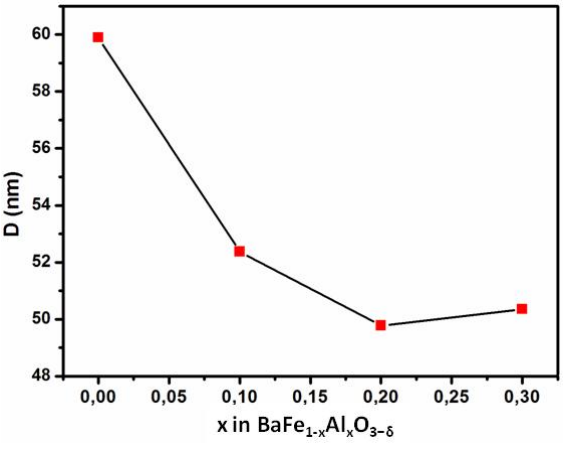

Fig. 7. Crystallite size of $BaFe_{1-x}Al_xO_{3-\delta}$ ($0.0 \le x \le 0.3$) samples

Table 2

Main textural properties of the $BaFe_{1-x}Al_xO_{3-\delta}$ samples

Sample	S_{BET}, $m^2 \cdot g^{-1}$	Total pore volume, $cc \cdot g^{-1}$	Average pore diameter, Å
$x = 0$	1.04	0.00255	97.919
$x = 0.1$	1.16	0.00247	85.244
$x = 0.2$	1.35	0.00292	95.157
$x = 0.3$	1.22	0.00248	73.278

The morphologies of the $BaFe_{1-x}Al_xO_{3-\delta}$ samples examined by SEM are shown in Fig. 9. The micrographs indicate that particles of different shapes and sizes were formed with very well pronounced agglomeration. It can be seen that particles did not show a distinct shape and the particle size is greater than 1 µm. The grain boundaries are compact and there is only very small amount of pores. The formation of agglomerates is probably due to the nature of the solvent used in the preparation of the gels. The same result was also found for samarium doped ceria powders [36] and $SrCo_{1-x}Ni_xO_{3-\delta}$ oxides [37]. It has been shown that treating the precipitate with water and ethanol allows interactions between particles, which lead during drying to the formation of chemical bonds.

3.5. Electrical Conductivity Measurements

The temperature dependence of the electrical conductivity of the $BaFe_{1-x}Al_xO_{3-\delta}$ (x = 0, 0.1, 0.2 and 0.3) compounds in the temperature range 298 K ≤ T ≤ 773 K are presented in Fig. 10. All samples exhibit the same tendency: the electrical conductivity increase with increasing temperature up to 773 K, which indicates the semiconducting behavior. The increase of the electrical conductivity with increasing temperature reflects the enhancement of the concentration of free electrons, holes and tetravalent Fe ions. This behavior is similar to that observed in Al-doped $SrFeO_3$ [38, 39]. The substitution of Fe by Al ions induces a decrease of the electrical conductivity compared to the non-substituted $BaFeO_{3-\delta}$ compound. The decrease in the electrical conductivity is associated with the decrease in Fe^{4+} content and charge carriers in the system. Since Al^{3+} cation have stable oxidation state. The same trends were found for $La_{0.3}Sr_{0.7}Fe_{1-x}Ga_xO_{2.65+\delta}$ [40], and $BaFe_{1-x}Ta_xO_{3-\delta}$ [41]. Nevertheless, it should be pointed out that the electrical conductivity of the polycrystalline $BaFe_{1-x}Al_xO_{3-\delta}$ phase shows similar tendency compared to our previous theoretical results [42].

Fig. 11 shows the Arrhenius plot of [ln(σ) *vs.* 1000/T] for $BaFe_{1-x}Al_xO_{3-\delta}$ samples sintered at 1123 K.

The activation energy of conduction was determined from the plot using the following expression derived for the small polaron mechanism [43]:

$$s = A\exp\left(-\frac{E_a}{kT}\right) \quad (2)$$

where E_a is the activation energy of the conduction process; k is the Boltzmann constant; T is the absolute temperature; A the pre-exponential factor.

The slope of the graph above enables the determination of the activation energy E_a. As seen from the curves, the data for all samples exhibits linear variations in the whole temperature range. The calculated activation energies for the major perovskite phase of 0.071, 0.066, 0.62, and 0.058 eV for x = 0, 0.1, 0.2 and 0.3, respectively, are closer to those reported in [44, 45]. It can be also noticed that the activation energy decreases with increasing Al content. This trend indicates that the bandwidth increases with increasing Al content [40].

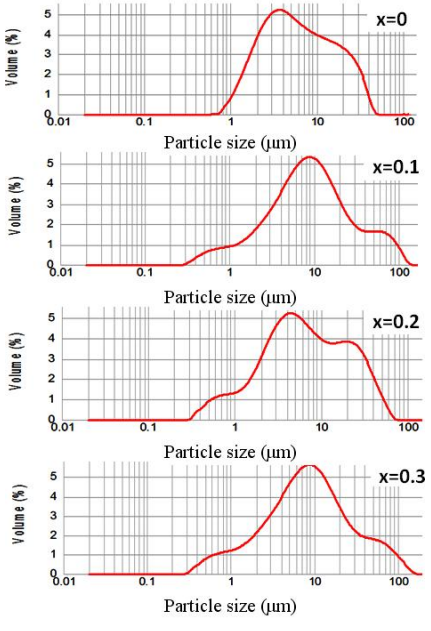

Fig. 8. Particle size distribution of the samples with x = 0, 0.1, 0.2 and 0.3

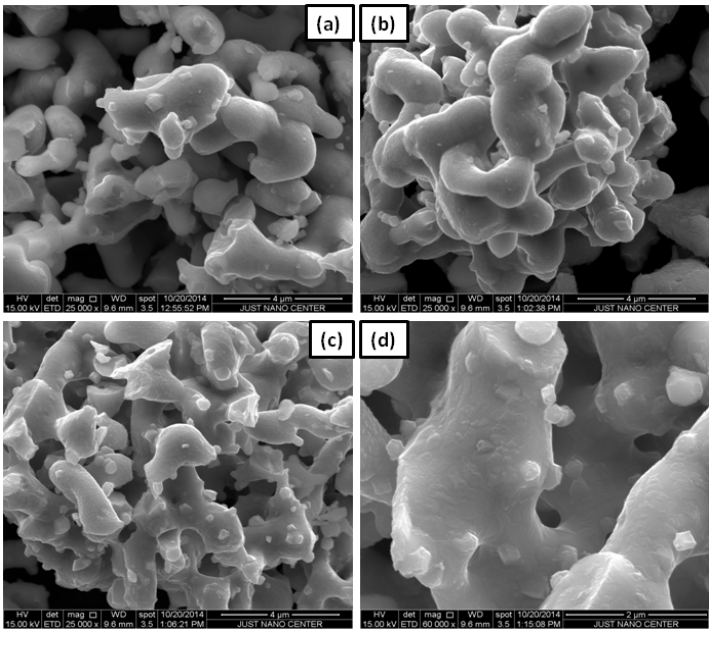

Fig. 9. SEM micrographs of $BaFe_{1-x}Al_xO_{3-\delta}$: x = 0 (a); x = 0.1 (b); x = 0.2 (c) and x = 0.3 (d) calcined at 1123 K

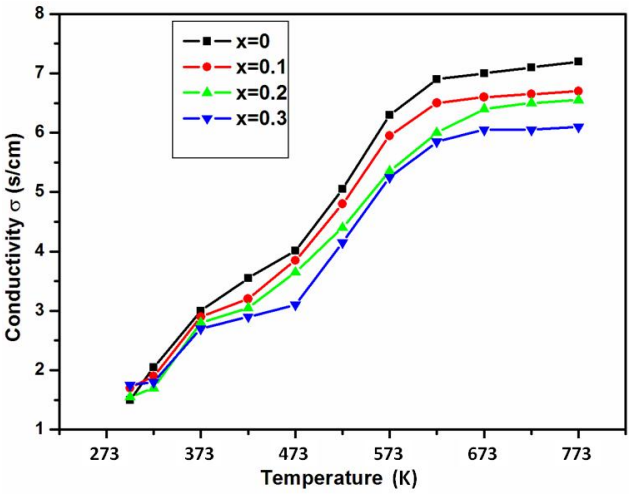

Fig. 10. Electrical conductivity of $BaFe_{1-x}Al_xO_{3-\delta}$ ($0.0 \leq x \leq 0.3$) as a function of temperatures

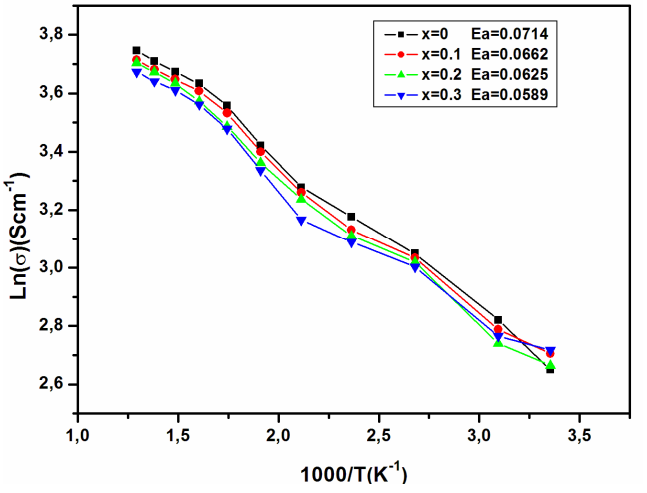

Fig. 11. Arrhenius plots of the $BaFe_{1-x}Al_xO_{3-\delta}$ (x = 0–0.3)

4. Conclusions

$BaFe_{1-x}Al_xO_{3-\delta}$ perovskite-type oxides in the composition range x = 0–0.3 were successfully synthesized by the citrate sol-gel method. TGA curve show the thermochemical behavior of the compound with respect to temperatures. XRD analysis of the decomposition of the precursors show that all samples crystallize with hexagonal structure at 1123 K, with a change to a rhombohedral perovskite at 1273 K, as well confirmed by IR spectroscopy. The textural properties of corresponding materials calcined at 1123 K have been explored by S_{BET} measurements and PSD analysis, demonstrating that the agglomeration degree of primary particles increases with increasing amount of aluminum, while the total pore volume shows a maximum for $BaFe_{0.8}Al_{0.2}O_{3-\delta}$. The microstructure and morphology of the compounds show that the powders are constituted by the aggregation of various dimensions and forms of particles. The electrical conductivity increases with increasing temperature, indicating a semiconductor-type behavior. The plot of ln(σ) against reciprocal temperature obeys the Arrhenius rule. The calculated activation energies for the major perovskite phase are of 0.071, 0.066, 0.62, and 0.058 eV for x = 0, 0.1, 0.2 and 0.3, respectively. Compared to all studied compositions, $BaFeO_{3-\delta}$ electrode exhibits greater electrical conductivity.

Acknowledgments

We wish to thank Professor B. A. Albiss, Jordan University of Science and Technology for carrying out electrical measurements.

References

[1] Goodenough J., Gräper W., Holtzberg F. *et. al.*: Landlot Börnstein Numerical Data and Functional Relationships in Science and Technology. Springer-Verlag, Berlin 1970.
[2] Galasso F.: Perovskite and High Tc Superconductors, Gordon and Breach Science Publishers, New York 1990.
[3] Weber A. and Ivers-Tiffee E.: J. Power Sources, 2004, **127**, 273.
[4] Hayashi H., Inaba H., Matsuyama M. *et al.*: Solid State Ionics, 1999, **1**, 122.
[5] Pena M. and Fierro J.: Chem. Rev., 2001, **101**, 1981.
[6] Grenier J., Wattiaux A., Pouchard M. *et al.*: J. Solid State Chem., 1989, **80**, 6.
[7] Nowik I., Herber R., Koltypin M. *et al.*: J. Phys. Chem. Solids, 2005, **66**, 1307.
[8] Yang Y., Jiang Y., Wang Y. and Sun Y.: J. Mol. Catal. A, 2007, **270**, 56.
[9] Pullar R. and Bhattacharya A.: Mater. Lett., 2002, **57**, 537.
[10] Dho J., Lee E., Park J. and Hur N.: J. Magn. Magn. Mater., 2005, **285**, 164.
[11] Aguadero A., Perez-Coll D., Calle C. *et al.*: J. Power Sources, 2009, **192**, 132.
[12] Sun M., Jiang Y., Li F. *et al.*: Mat. Res. Bull., 2011, **46**, 801.
[13] Lu C., Hu C. and Wu C.: Mater. Lett., 2007, **61**, 3959.
[14] Li F., Liu Y., Liu R. *et al.*: Mater. Lett., 2010, **64**, 223.
[15] Suvegh K., Nomura K., Juhasz G. *et al.*: Radiat. Phys. Chem., 2000, **58**, 733.
[16] Kharton V., Yaremchenko A., Viskup A. *et al.*: J. Electrochem. Soc., 2002, **149**, 125.
[17] Kharton V., Shaulo A., Viskup A. *et al.*: Solid State Ionics, 2002, **150**, 229.
[18] Leonidov I., Kozhevnikov V., Mitberg E. *et al.*: J. Mater. Chem., 2001, **11**, 1201.
[19] Lebid M. and Omari M.: Arab. J. Sci. Eng., 2014, **39**, 147.
[20] Xian H., Zhang X., Li X. *et al.*: J. Catal. Today, 2010, **158**, 215.
[21] Rida K., Pena M., Sastre E. and Martinez-Arias A.: J. Rare Earths, 2012, **30**, 210.
[22] Yang Y., Jiang Y., Wang Y. and Sun Y.: J. Catal. A, 2007, **270**, 56.

[23] Ge C., Li L., Xian H. *et al.*: J. Fuel Process. Technol., 2014, **120**, 1.
[24] Shotaro M., Kaori K. and Saburo N.: J. Magn. Magn. Mater., 2004, **272**, 127.
[25] Nowik I., Herber R., Koltypin M. *et al.*: J. Phys. Chem. Solids, 2005, **66**, 1307.
[26] Yoon S. and Kim C.: J. Appl. Phys., 2005, **10A**, 318.
[27] Bellakki M. and Manivannan V.: J. Das Mater. Res. Bull., 2009, **44**, 1522.
[28] Falcon H., Carbonio R. and Fierroy J.: J. Catal., 2001, **203**, 264.
[29] Shannon R.: Acta Crystallogr. Sect., 1976, **32A**, 751.
[30] Khalil M.: Mat. Sci. Eng., 2003, **64**, A352.
[31] Sun M., Jiang Y., Li F. *et al.*: J. Mater. Trans., 2010, **51**, 1981.
[32] Cullity B.: Elements of X-ray Diffractions. Addison Wesley Publ., Massachusetts 1978.
[33] Tulloch J. and Donne S.: J. Power Sources, 2009, **188**, 359.
[34] Mota N., Alvarez-Galvana M., Navarroa R. *et al.*: Appl. Catal. B, 2012, **113**, 271.
[35] Tejuca L. and Fierro J.: Therm. Acta, 1989, **147**, 361.
[36] Jung G., Huang T., Huang M. and Chang C.: J. Mater. Sci., 2001, **36**, 5839.
[37] Makhloufi S. and Omari M.: J. Inorg. Organomet. Polym., 2016, **26**, 32.
[38] Yasuda I. and Hikita T.: J. Electrochem. Soc., 1993, **140**, 1699
[39] Kamata H., Yononemura Y., Mizusaki J. *et al.*: J. Phys. Chem. Solids, 1995, **56**, 943.
[40] Yaremchenko A., Patrakeeva M., Khartona V. *et al.*: Solid State Sci., 2004, **6**, 357.
[41] Bektasa M., Kamina D., Hagena G. *et al.*: J. Sens. Actuators, 2014, **208**, B190.
[42] Hanane F. and Kaouther El.: Int. J. Eng. Innovat. Technol. (IJEIT), 2014, **3**, 9.
[43] Lu S., Yu B., Meng X. *et al.*: J. Power Sources, 2015, **273**, 24.
[44] Kharton V., Kovalevsky A., Tikhonovich V. *et al.*: Solid State Ionics, 1998, **110**, 53.
[45] Xiao G., Liu Q., Wang S. *et al.*: J. Power Sources, 2011, **11**, 21.

СИНТЕЗ, СТРУКТУРНІ І ФІЗИКО-ХІМІЧНІ ХАРАКТЕРИСТИКИ $BaFe_{1-x}Al_xO_{3-d}$

Анотація. *За допомогою золь-гель методу з використанням лимонної кислоти як хелатного агента отримано оксиди* $BaFe_{1-x}Al_xO_{3-\delta}$ $(0 \le x \le 0.3)$ *зі структурою типу перовскіту. Досліджено вплив температури прокалювання на фізико-хімічні властивості оксиду. За допомогою термогравіметричного аналізу, Фур'є інфрачервоної спектроскопії та рентгенівської дифракції вивчено розклад прекурсора і визначено адекватну температуру прокалювання для отримання нанопорошків. Встановлено, що за температури 1123 K сполуки мають гексагональну кристалічну структуру. Зразки, отримані після прокалювання при 1123 K, досліджено за допомогою рентгенівської дифракції, аналізу Брунауера-Еммета-Теллера (БЕТ), скануючої електронної мікроскопії та визначено їх електропровідність. Мікроструктурними і морфологічними дослідженнями встановлено, що частинки мають практично сферичну форму і частково агломеруються. Показано, що найбільшу площу поверхні і загальний об'єм пор має оксид* $BaFe_{0.8}Al_{0.2}O_{3-\delta}$. *Напівпровідниковий характер доведений температурною залежністю електропровідності.*

Ключові слова: *оксид перовскіту, БЕТ, золь-гель метод, порошкова дифракція, електропровідність.*